Supporting Information

Su et al. 10.1073/pnas.1100369108

SI Text

The dimensions of odor delivery systems (including flow rates and tube sizes) have been shown to affect the stimulus shape (1). The dimensions are constants of the configurations used here and have been chosen to optimize the stimulus shape and setup versatility within the limits imposed by the instrumentation for electrophysiology. In both configurations, a main air stream of charcoal-filtered air (2,000 mL/min) is directed at the fly through a glass tube (5 mm). The fly is positioned at ∼1 cm from the mouth of the odor delivery tube. A secondary air stream (200 mL/min) is then added to the main air stream through an opening on the side of the glass odor delivery tube. A suction tube (9,600 mL/min, diameter ∼8 cm) is placed at ∼5 cm from the fly on the opposite side. All molecules with ionization potential below 10.6 eV can be ionized and thus detected by the photoionization detector (PID). The PID suction rate was 660 mL/min. The analog PID output (0–10 V) is acquired in LabVIEW (National Instruments) using NI-USB-6211 data acquisition module. Routine calibration and maintenance was carried out to ensure PID reproducibility. Calibration curves and response functions of individual odorants used in the current study were not measured because of technical difficulties in determining the exact odor vapor concentrations and producing fast-varying stimuli (>1,000 Hz). We used PID to measure the dynamics of odorants delivered in the following two odor delivery systems.

i) Odor cartridge downstream of the valve (Fig. S7*A*). This is the configuration used for most of the electrophysiological recordings in this study. Fifty microliters of odor dilution was added to a paper filter disk positioned in a Pasteur pipette. A three-way solenoid valve controls and allows the secondary air stream into the pipette. The stimulus is delivered by manually inserting the tip of the pipette in the hole of the glass tube carrying the main humidified air stream. Stimuli are of 500 ms unless specified otherwise, and the same odorant-containing pipette is used at most four times.

ii) Odor bottle upstream of the valve (Fig. S7*B*). Two three-way solenoid valves are inserted into the glass odor delivery tube at a position 5 cm from the downstream end of the odor delivery tube. A clean air stream (200 mL/min) flows continuously through valve #1 (v1), which usually stays open. A second air stream (200 mL/min) flows first into a bottle containing 20 mL of odor dilution and then through valve #2 (v2), which is usually closed so that the odor stream is directed to an exhaust tube. This allows odor vapor to equilibrate with the liquid phase and the air stream. The two valves switch on and off simultaneously so that either the clean air stream or the odor stream is added to the main flow. To prevent contamination, we used new valves and tubings for each odor tested.

To test whether different odor delivery systems influence the shape of odor stimuli, we took PID measurements of linalool and methyl butyrate using the above-mentioned odor delivery configurations. As shown in the main text, when a 500-ms pulse of odor is delivered via an odor cartridge (Fig. S7*A*), the PID response to linalool showed a slower rising (and decay) phase compared with that of methyl butyrate (Fig. S7*C*). This difference in the rising phase between the two odorants persisted when the stimulus was delivered using a bottle upstream of the valves (Fig. S7*D*).

We note that, although methyl butyrate gas-phase concentration at 10^{-3} dilution (measured as PID peak response, which is not shown) is similar using either odor delivery configuration (Fig. S7), pure linalool was required when delivered from an odor bottle (Fig. S7*B*) to obtain a PID response comparable to a 10^{-2} dilution using an odor cartridge. This difference may be attributed to the different saturated vapor pressures of the two odorants.

1. Vetter RS, Sage AE, Justsus KA, Cardé RT, Galizia CG (2006) Temporal integrity of an airborne odor stimulus is greatly affected by physical aspects of the odor delivery system. *Chem Senses* 31:359–369.

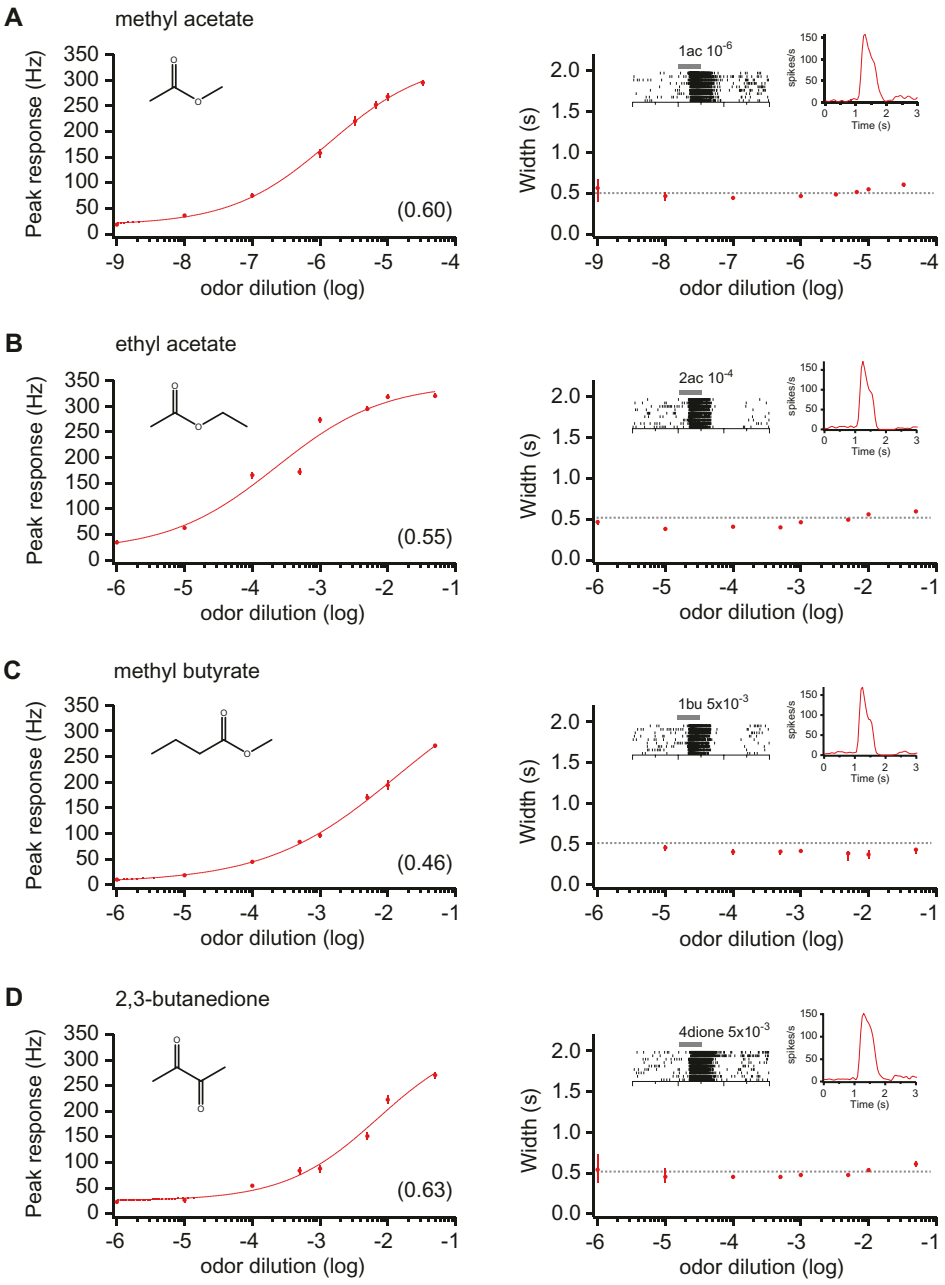

Fig. S1. Excitatory responses of ab2A. (*A–D*) Four different strong excitatory odorants over a wide concentration range were presented as 500-ms puffs to ab2A ORNs. Peak responses (*Left* panels) and the width of the response (*Right* panels) were plotted as a function of odorant concentration ($n = 9$). Error bars: ± SEM (*Left* panels); variations in width are due to SEM (*Right* panels). Dose–response relationships were fitted with the Hill equation. Hill coefficients are indicated in parentheses. (*Insets*) Raster plots and the corresponding peri-stimulus time histograms of sample responses of similar magnitude, binned at 50 ms. The response magnitude, not width, changed with odorant concentrations at subsaturating concentrations.

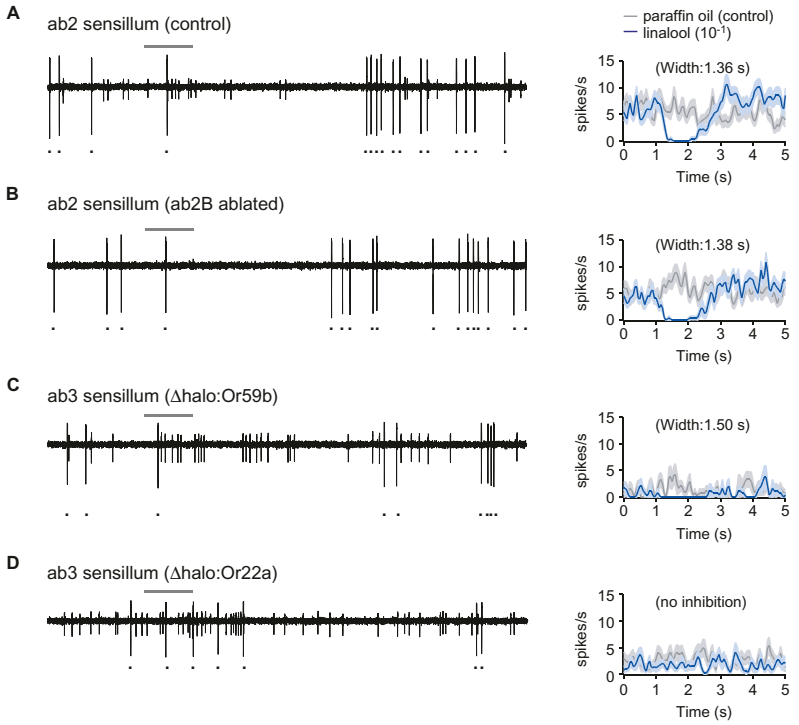

Fig. S2. Linalool inhibition does not depend on the ab2B neuron and is conferred by the ab2A receptor. (*Left* panels) Sample traces of single-unit recordings, showing olfactory responses of the A neurons (larger spikes, marked by black dots) to a 500-ms pulse of linalool (gray bar). (*Right* panels) PSTHs of the A neuron responses to the solvent control, paraffin oil (gray traces), and to linalool (blue traces), spikes binned in 50-ms intervals. Shaded area: ±SEM. (*A*) Recordings from ab2 sensilla containing both ab2A and ab2B ORNs (n = 24). The B neuron has a smaller spike amplitude. (*B*) Recordings from ab2 sensilla in which the ab2B neurons were genetically ablated. Ablation was achieved using a *GAL4* construct to drive *UAS-reaper*, which can be seen to eliminate ab2B spiking (n = 24; Table S1). (*C*) Recordings from mutant (*Δhalo*) ab3 sensilla in which the endogenous receptor in the ab3A neuron was replaced with Or59b, the receptor normally expressed in the ab2A neuron (n = 12). (*D*) Recordings from mutant (*Δhalo*) ab3 sensilla in which ab3A expressed another receptor, Or22a (n = 24). Linalool inhibited ab2A independently of the presence of the neighboring ORN (*B*) and is conferred by the ab2A receptor (*C*).

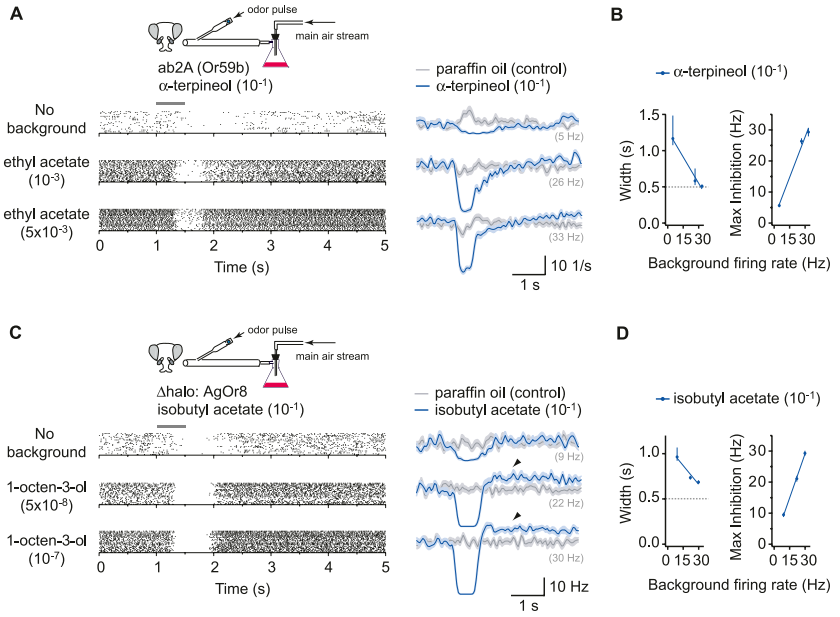

Fig. S3. Other inhibitory responses with background excitation. Raster plots and the corresponding PSTHs of ab2A ORNs (*A*) and mutant ab3A ORNs expressing AgOr8 (*C*) in response to a 500-ms pulse of inhibitory odorant (gray bars) in the absence or presence of a background excitatory odorant. Gray traces: solvent control, paraffin oil; blue traces: inhibitory odorant (n = 24). The average prestimulus background firing rates are indicated in parentheses in gray (n = 24). Arrowhead: rebound response. (*B* and *D*) Average width of the inhibitory responses (Width) and the magnitude of peak inhibition (Max Inhibition, minimum response subtracted from average background firing rate) plotted as a function of background firing rate. Error bars: variations in width due to SEM (Width); ±SEM (Max Inhibition). Dotted lines: duration of the odor pulse, 500 ms.

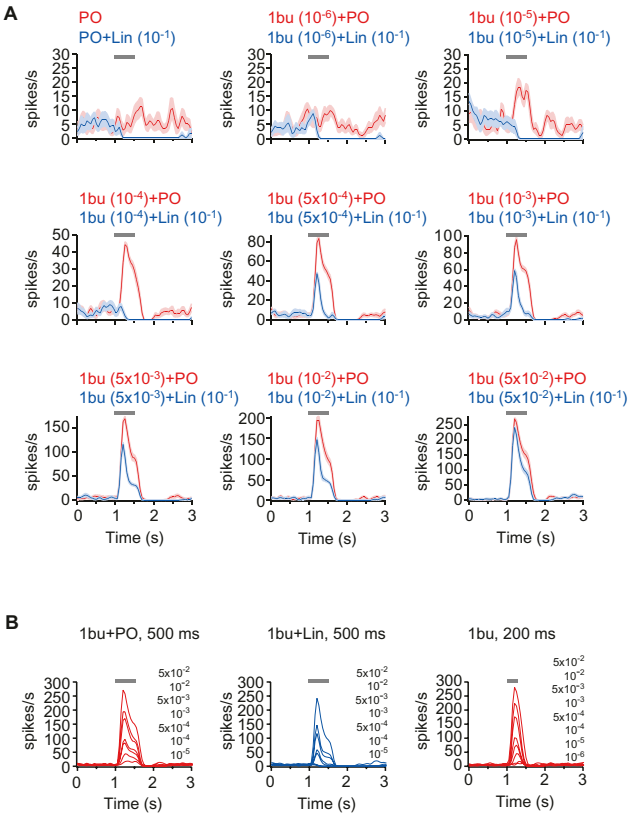

Fig. S4. Comparison of ab2A response dynamics. (*A*) PSTHs of ab2A ORNs in response to a 500-ms pulse of a binary odor mixture containing equal parts of methyl butyrate (1 bu) at increasing concentrations and linalool (Lin) or paraffin oil (PO). (*B*) PSTHs of ab2A ORNs in response to a 500-ms (*Left* and *Center*) or a 200-ms (*Right*) pulse of odor stimulus, containing methyl butyrate or a methyl butyrate/linalool mixture ($n = 9$). Methyl butyrate dilutions are indicated on the right in each panel in *B*.

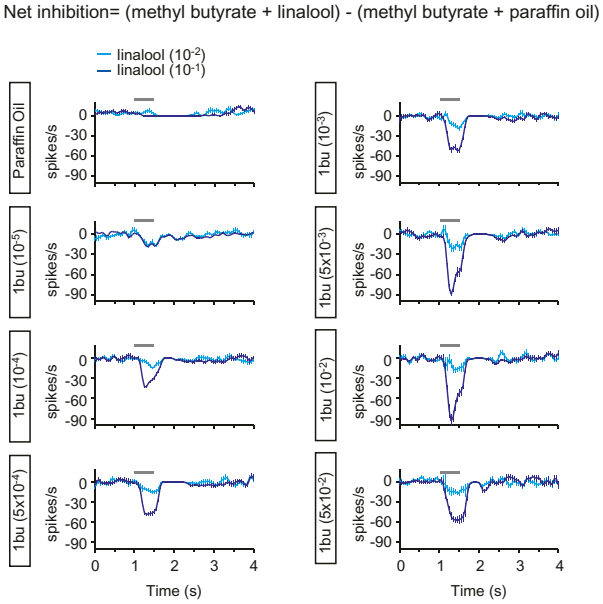

Fig. S5. The net effects of an inhibitory odorant in a mixture. The net effects of linalool inhibition in a binary mixture on ab2A responses were obtained by subtracting the control responses (methyl butyrate mixed with paraffin oil) from the responses to methyl butyrate mixed with linalool. Methyl butyrate (1 bu) dilutions are indicated on the left in each panel.

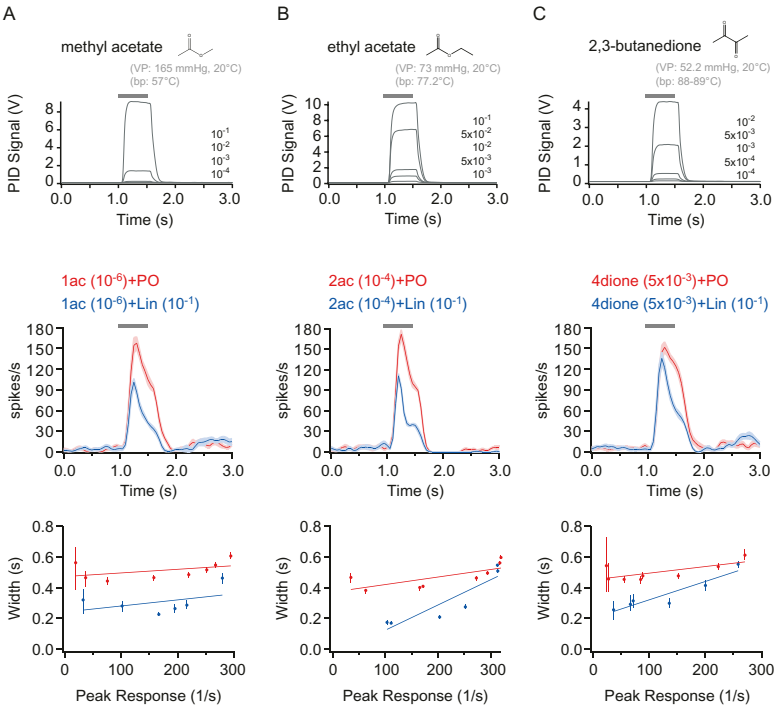

Fig. S6. Three additional ab2A excitatory odorants. (*Top*) PID measurements of three different ab2A excitatory odorants: methyl acetate (*A*), ethyl acetate (*B*), and 2,3-butanedione (*C*). (*Middle*) PSTHs of ab2A ORNs in response to a 500-ms pulse of a binary odor mixture containing equal parts of the excitatory odorant and linalool (Lin) or paraffin oil (PO). (*Bottom*) Response width as a function of the peak response with different concentrations of the excitatory odorants.

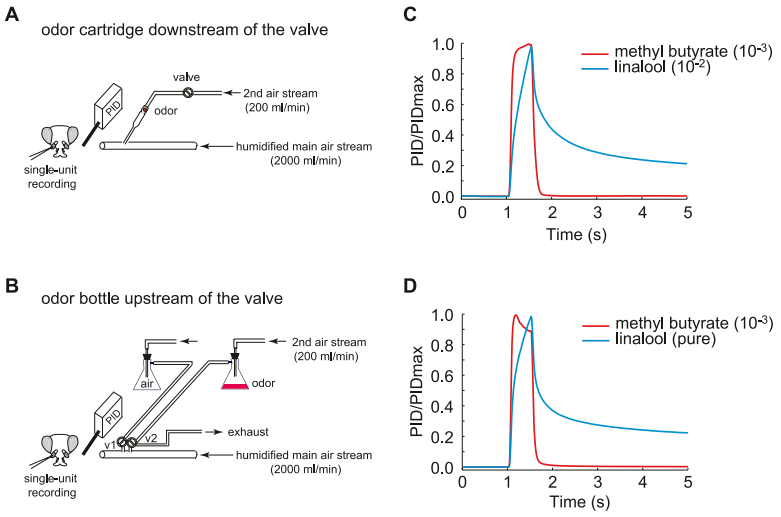

Fig. S7. Comparison of odor delivery systems. Illustrations of two commonly used odor delivery systems (*A* and *B*) and the respective normalized PID measurements of the fast and slow odorants, methyl butyrate and linalool (*C* and *D*). The drawings are not to scale. The valves shown (*B*) are very close to the side opening of the odor delivery tube. The systems are described in *SI Text*.

Table S1. Fly genotypes

	Genotypes of the analyzed flies
Fig. 1	CS
Fig. 2	CS
Fig. 3	CS
Fig. 4	*w;Δhalo/Δhalo; Or22a-GAL4/UAS-AgOr1*
Fig. S1	CS
Fig. S2*A*	CS
Fig. S2*B*	*w; UAS-rpr; Gr43a-GAL4*
Fig. S2*C*	*w;Δhalo/Δhalo; Or22a-GAL4/UAS-Or59b*
Fig. S2*D*	*w;Δhalo/Δhalo; Or22a-GAL4/UAS-Or22a*
Fig. S3*A*	CS
Fig. S3*B*	*w;Δhalo/Δhalo; Or22a-GAL4/UAS-AgOr8*
Fig. S4	CS
Fig. S5	CS
Fig. S6	CS

Table S2. PID measurements of different odorants

Odorant	Dilution	PID peak	τ_{on}	τ_{on_min}	τ_{on_max}	A	A_{min}	A_{max}
Methyl acetate	10^{-4}	0.0164	0.0287	0.0284	0.0290	0.0148	0.0147	0.0148
	10^{-3}	0.1483	0.0321	0.0321	0.0322	0.1399	0.1398	0.1400
	10^{-2}	1.3738	0.0325	0.0323	0.0327	1.3244	1.3230	1.3260
	10^{-1}	9.1182	0.0304	0.0302	0.0306	9.1122	9.1020	9.1130
Ethyl acetate	10^{-3}	0.2272	0.0375	0.0373	0.0376	0.2048	0.2047	0.2050
	5×10^{-3}	1.0419	0.0341	0.0340	0.0342	0.9941	0.9937	0.9946
	10^{-2}	2.1581	0.0325	0.0323	0.0326	1.9839	1.9830	1.9850
	5×10^{-2}	7.9946	0.0266	0.0265	0.0268	7.7645	7.7600	7.7690
Methyl butyrate	10^{-4}	0.0160	0.0644	0.0639	0.0648	0.0142	0.0142	0.0143
	5×10^{-4}	0.0415	0.0539	0.0537	0.0541	0.0383	0.0383	0.0383
	10^{-3}	0.0774	0.0484	0.0482	0.0485	0.0735	0.0734	0.0736
	5×10^{-3}	0.3803	0.0468	0.0466	0.0470	0.3508	0.3505	0.3511
	10^{-2}	0.7224	0.0424	0.0422	0.0426	0.6601	0.6595	0.6606
2,3-Butanedione	5×10^{-4}	0.1408	0.0243	0.0241	0.0245	0.1371	0.1370	0.1373
	10^{-3}	0.4345	0.0234	0.0233	0.0235	0.4303	0.4301	0.4305
	5×10^{-3}	2.0725	0.0336	0.0336	0.0337	1.9760	1.9750	1.9770
	10^{-2}	4.5218	0.0291	0.0290	0.0291	4.2750	4.2740	4.2760
Linalool	3×10^{-3}	0.0131	0.5358	0.5246	0.5470	0.0215	0.0212	0.0219
	10^{-2}	0.1261	0.3100	0.3076	0.3123	0.1494	0.1488	0.1501
	3×10^{-2}	0.3555	0.2564	0.2548	0.2580	0.3978	0.3966	0.3991
	10^{-1}	0.7048	0.1719	0.1713	0.1726	0.7336	0.7325	0.7347
4-Methylphenol	10^{-3}	0.0068	0.4219	0.4126	0.4311	0.0092	0.0091	0.0094
	5×10^{-3}	0.1074	0.3580	0.3574	0.3587	0.1406	0.1404	0.1408
	10^{-2}	0.2462	0.3106	0.3097	0.3115	0.2964	0.2959	0.2969
	5×10^{-2}	0.4642	0.2959	0.2950	0.2968	0.5586	0.5576	0.5595
6-Methyl-5-hepten-2-one	10^{-3}	0.0392	0.1988	0.1973	0.2000	0.0395	0.0394	0.0396
	10^{-2}	0.3953	0.1203	0.1198	0.1208	0.3929	0.3924	0.3934
	10^{-1}	2.5987	0.0729	0.0724	0.0734	2.4562	2.4520	2.4600

The rising phase was fitted with the exponential curve $y(t) = A^*\exp(-t/\tau_{on})$. Minimum and maximum values for τ_{on} and A are the lower and upper confidence bounds for a 95% confidence level as computed in MATLAB using a Student's t test cumulative distribution algorithm.